http://www.diva-portal.org

Postprint

This is the accepted version of a paper published in *Protein Science*. This paper has been peer-reviewed but does not include the final publisher proof-corrections or journal pagination.

Citation for the original published paper (version of record):

Thomaeus, A., Naworyta, A., Mowbray, S., Widersten, M. (2008)
Removal of distal protein-water hydrogen bonds in a plant epoxide hydrolase increases catalytic turnover but decreases thermostability.
Protein Science, 17(7): 1275-1284
http://dx.doi.org/10.1110/ps.034173.107

Access to the published version may require subscription.

N.B. When citing this work, cite the original published paper.

Permanent link to this version:
http://urn.kb.se/resolve?urn=urn:nbn:se:uu:diva-17590

Removal of distal protein-water hydrogen bonds in a plant epoxide hydrolase increases catalytic turnover but decreases thermostability

Ann Thomaeus[1], Agata Naworyta[2], Sherry L. Mowbray[2] & Mikael Widersten[1, *]

[1]Department of Biochemistry and Organic Chemistry, Uppsala University, Box 576, Biomedical Center, SE-751 23 Uppsala, Sweden

[2]Department of Molecular Biology, Swedish University of Agricultural Sciences, Box 590, Biomedical Center, SE-751 24 Uppsala, Sweden

[*]Corresponding author. E-mail: mikael.widersten@biorg.uu.se, Phone: +46 (0)18 471 4992, Fax: +46 (0)18 55 8431.

Running title: Protein-water hydrogen bonds in epoxide hydrolase

No of pages: 28 + 8 figures

Abstract

A putative proton wire in potato soluble epoxide hydrolase 1, StEH1, was identified and investigated by means of site-directed mutagenesis, steady state kinetic measurements, temperature inactivation studies, and x-ray crystallography. The chain of hydrogen bonds includes five water molecules coordinated through backbone carbonyl oxygens of Pro^{186}, $Leu^{266,}$ His^{269}, and the His^{153} imidazole. The hydroxyl of Tyr^{149} is also an integrated component of the chain, which leads to the hydroxyl of Tyr^{154}. Available data suggest that Tyr^{154} functions as final proton donor to the anionic alkylenzyme intermediate formed during catalysis. To investigate the role of the putative proton wire, mutants Y149F, H153F, and Y149F/H153F, were constructed and purified. The structure of the Y149F mutant was solved by molecular replacement and refined to 2.0 Å resolution. Comparison with the structure of wild-type StEH1 revealed only subtle structural differences. The hydroxyl group lost as a result of the mutation was replaced by a water molecule, thus maintaining a functioning hydrogen bond network in the proton wire. All mutants showed decreased catalytic efficiencies with the *R,R*-enantiomer of *trans*-stilbene oxide whereas with the *S,S*-enantiomer k_{cat}/K_M was similar or slightly increased as compared to the wild-type reactions. k_{cat} for the Y149F mutant with either TSO enantiomer was increased; thus the lowered enzyme efficiencies were due to increases in K_M. Thermal inactivation studies revealed that the mutated enzymes were more sensitive to elevated temperatures than the wild-type enzyme. Hence, structural alterations affecting the hydrogen bond chain caused increases in k_{cat} but lowered thermostability.

Keywords: epoxide hydrolase, proton wire, thermostability, mutants, x-ray crystal structure

Abbreviations used: StEH1, epoxide hydrolase 1 from *Solanum tuberosum*; TSO, *trans*-stilbene oxide; PEG, polyethylene glycol; HEPES, 4-(2-hydroxyethyl)-1-piperazineethanesulfonic acid.

Soluble epoxide hydrolases (EC 3.3.2.10) are cofactor-independent enzymes belonging to the α/β-hydrolase fold superfamily (Ollis et al. 1992). The reaction catalyzed is the hydrolytic ring opening of an epoxide to form the corresponding vicinal diol (Fig. 1). Epoxide hydrolases show high catalytic activity as well as high enantioselectivity, which make them suitable for further development into specific and efficient biocatalysts (Archelas and Furstoss 2001; Koeller and Wong 2001; Steinreiber and Faber 2001). Such enzymes are widespread in nature; they are present in organisms from all kingdoms, with a variety of assigned functions. In some organisms, including humans, epoxide hydrolases function as detoxification enzymes, converting potentially harmful epoxides into less toxic and more easily excretable diol products. It has further been shown that human soluble epoxide hydrolase is a promising therapeutic target in ischemic stroke and is associated with hypertension-related kidney damage and systemic inflammation (Zhao et al. 2004; Imig 2005; Schmelzer et al. 2005; Zhang et al. 2007). Other known functions of epoxide hydrolases are in secondary catabolism and in regulation of signal molecules. In plants, epoxide hydrolases have been proposed to be involved in pathogen defense by participating in the synthesis of cutin (Kolattukudy 1981; Fauth et al. 1998; Arand et al. 2003; Morrisseau and Hammock 2005).

The simplest view of the catalyzed hydrolysis encompasses four steps, illustrated for the model substrate *trans*-stilbene oxide (TSO) in Fig. 1. Formation of the enzyme-substrate complex is followed by nucleophilic attack by an active-site aspartate carboxylate, which generates a covalent alkylenzyme intermediate. A general base-activated water reacts with the covalent intermediate and the diol product is formed. Product release completes a cycle of catalytic turnover (see Armstrong and Cassidy 2000, for a review).

Central structural features of the epoxide hydrolase fold are a core α/β domain and a mainly α-helical lid domain. A catalytic triad, consisting of the Asp nucleophile, His general base and an Asp charge relay residue, is located on the α/β domain, while two key tyrosyl residues are placed on the lid. In StEH1, a soluble monomeric epoxide hydrolase from potato, these catalytic groups are contributed by Asp^{105} as nucleophile, His^{300} as general base, Asp^{265} as charge relay residue and the Tyr^{154}/Tyr^{235} pair (Elfström and Widersten 2005, 2006). From the x-ray crystal structure of StEH1 (PDB entry code 2CJP; Mowbray et al. 2006) an additional catalytic residue, Glu^{35}, was identified. This residue has been shown to be important, both in the activation of Asp^{105} and in the hydrolysis half-reaction, in the latter case by properly orienting the water molecule that attacks the alkylenzyme intermediate (Thomaeus et al. 2007). Strong conservation regarding both structure and chemical functionality is found between the potato enzyme and other plant isoenzymes. Conservation of the key catalytic residues extends also to the mammalian soluble epoxide hydrolases (Thomaeus et al. 2007). The combined data allow some general conclusions to be drawn regarding structure/function relationships in the entire enzyme family. For instance, the attack of the base-activated water molecule is proposed to take place in concert with protonation of the negatively charged alkylenzyme intermediate. The proton is suggested to be transferred from donor oxonium ions of the bulk solvent through a chain of water molecules that leads to the active-site Tyr^{154} (Elfström and Widersten 2006), originally identified in the StEH1 crystal structure (Mowbray et al. 2006). The waters in the protein tunnel are coordinated by the following residues of the enzyme (listed in consecutive order, proceeding from the active site in the interior to the protein surface): the hydroxyl group of Tyr^{154}, the imidazole moiety of His^{153}, the backbone carbonyl of Leu^{266}, the hydroxyl of Tyr^{149}, the backbone carbonyl of His^{269}, and finally, the backbone

carbonyl of Pro^{186} (Fig. 2). The hydroxyl groups of tyrosines 149 and 154 can be viewed as integral components of the chain (Fig. 2). To assess the importance and role of this putative proton wire, three mutants of StEH1, Y149F, H153F, and Y149F/H153F, were constructed and expressed in *Escherichia coli*, allowing their functional properties to be compared with those of the wild-type enzyme. In addition, the x-ray crystal structure of mutant Y149F was determined to evaluate any structural effects caused by the mutation.

Results

Site-directed mutagenesis, protein expression, and purification

The single mutants of StEH1, Y149F and H153F, and the double mutant Y149F/H153F, were constructed using plasmid pGTacStEH1-5H, coding for wild-type StEH1, as cDNA template, together with mutagenic primers in the polymerase chain reactions. The enzymes, both wild type and mutants, were expressed in *E. coli* XL1-Blue and purified to homogeneity according to established procedures (Elfström and Widersten 2005) with comparable yields (20 mg/liter batch cultures). Purified proteins were stored at 4 °C and retained unchanged enzyme activity during the time of experimental data collection.

Structure of mutant Y149F

The structure of the substrate-free form of the StEH1 Y149F mutant at pH 7.5 was solved by molecular replacement using the wild-type protein structure (PDB entry code 2CJP) as a search model, and subsequently refined to a resolution of 2 Å. Statistics concerning data collection and refinement are shown in Table 1. Electron density in the region of interest is shown in Fig. 3A. Comparison with the wild-type

structure indicated that the Y149F point mutation led only to subtle changes; the two molecules in each respective asymmetric unit had an RMSD of 0.2 Å when all Cα atoms were compared. When the site of mutation is inspected, it becomes clear that removing the hydroxyl group of the wild-type tyrosyl residue results in a space that is filled by a water molecule (Fig. 3B). The other water molecules of the putative proton wire coordinate to the protein in essentially the same way as in the wild-type enzyme. The same water coordination is observed in both protein molecules in the asymmetric units of wild type and Y149F mutant structures.

Enzyme kinetics

The steady state parameters for the hydrolysis of both enantiomers of *trans*-stilbene oxide (TSO) were collected at 30 ºC and pH 6.8, the previously determined pH optimum for the wild-type enzyme (Elfström and Widersten 2005). In addition, the rate constants for formation (k_2) and decomposition (k_{-2} and k_3) of the alkylenzyme intermediate were determined for the Y149F catalyzed hydrolysis and compared to data for the wild-type enzyme. The results are listed in Tables 2 and 3 and commented on below. The data for the wild-type enzyme were collected under identical conditions as those for the mutants and were reproducible between enzyme batches.

Y149F mutant – For the reaction with *R,R*-TSO, both the k_{cat} and K_M parameters were elevated 1.9 to 3.6-fold, respectively, as compared to the wild-type catalyzed reaction. The resulting catalytic efficiency was half that exhibited by the wild-type enzyme. For the reaction with *S,S*-TSO, k_{cat} and K_M were only slightly increased and the k_{cat}/K_M parameter was not significantly changed. The observed rates (k_{obs}) for transient buildup of the alkylenzyme intermediate, reflected by quenching of intrinsic

tryptophan fluorescence (Elfström and Widersten 2006), displayed substrate concentration dependencies that allowed for determination of k_2, k_{-2} and k_3, and the equilibrium dissociation constant of the Michaelis complexes, K_S, as described in the methods section (Fig. 4). In the reaction with *R,R*-TSO, however, enzyme saturation was not reached within the solubility range of the substrate, and so values for K_S, k_2, k_{-2} and k_3, could not be determined with high accuracies.

However, it is clear from the results that the increases in k_{cat} displayed by the Y149F mutant with either TSO enantiomer can be linked to higher hydrolysis rates (k_3) underlining this step as primarily rate limiting. In the *S,S*-TSO reaction, the alkylenzyme formation rate was increased 2-fold while k_{-2} and K_S were essentially unchanged by the mutation.

H153F mutant – With *R,R*-TSO as substrate, the k_{cat} parameter was essentially unchanged as compared to the wild-type reaction, while K_M was 9-fold higher, resulting in a 15-fold drop in catalytic efficiency. With the *S,S*-enantiomer, k_{cat} and K_M were both increased 2- to 3-fold in a compensatory manner, resulting in a virtually unchanged k_{cat}/K_M.

Y149F/H153F mutant – With the double mutant, the hydrolysis of *R,R*-TSO presented experimental difficulties due to the inability to reach enzyme saturation within the solubility range of the substrate (≤ 80 µM). Hence, the k_{cat} and K_M parameters could not be determined individually. However, the turnover rate was not severely affected, as judged by the observed rate at the highest substrate concentration (> 10 s^{-1}). The catalytic efficiency could be accurately determined and showed a more than 10-fold decrease as compared to the corresponding wild-type value. $k_{cat}^{S,S\text{-TSO}}$ was increased while $K_M^{S,S\text{-TSO}}$ was virtually unaffected, thus resulting in a 2-fold elevated catalytic efficiency; $k_{cat}/K_M^{S,S\text{-TSO}}$ was 11-fold higher than the corresponding

value for *R,R*-TSO. For the wild-type enzyme, *R,R*-TSO was the slightly preferred substrate, while the double mutant had a strong preference for the *S,S*-enantiomer; the difference in enantiospecificity between the wild-type enzyme and the Y149F/H153F mutant was thus 33-fold.

pH dependence of catalysis

The pH dependence of k_{cat} for the Y149F mutant was determined with the procedure previously used for the wild-type StEH1 (Elfström and Widersten 2005); the results are shown in Fig. 5. The pH dependence of k_{cat} reflects the titration of ionizable groups from the enzyme-substrate complex through the alkylenzyme intermediate leading to product and titrates with a bell-shaped profile in the wild-type enzyme. The observed titration profiles of k_{cat} of the Y149F mutant suggested similar pH dependencies to the wild-type StEH1.

Thermostability of activity

The catalytic activities of the reactions with *R,R*-TSO in the presence of wild-type StEH1, Y149F, H153F or Y149F/H153F, following incubation of the enzymes at 55 °C, were determined. The wild-type activity was the most stable at this temperature, with an estimated half-life of two hours and fifteen minutes (Fig. 6A). The activities of the single mutants showed intermediate half-lives, one hour at 55 °C, whereas the double mutant exhibited a dramatic drop in enzyme activity, with an interpolated half-life of only 20 minutes. The effects on thermal inactivation appears to be additive; the sum of the inactivation times for each single mutant gives a good approximation of the sensitivity exhibited by the double mutant. The observed temperature inactivation was not reversible. Wild-type StEH1 was also more resistant to thermal inactivation

than the Y149F mutant in a temperature range between 55 °C and 64 °C. The wild type retained approximately 65% activity after five minutes incubation at 60 °C while, under the same conditions, the Y149F mutant had lost 70% of its initial activity at 30 °C (Fig. 6B). Hence, the results of the thermal inactivation of wild type and Y149F mutant after fixed-time incubations at varying temperatures are in agreement with the results from the study of time-dependent temperature inactivation following incubations at 55 °C.

Discussion

Proton transport can be accomplished by a continuous chain of hydrogen bonds, which may consist of protein functional groups or a combination of both protein and water (Nagle and Morowitz 1978). Proton wires made up only of water molecules occur in various types of proteins, ranging from transmembrane pores and thiamine-dependent enzymes to photosynthetic reaction centers (Pomès and Roux 1998; Frank et al. 2004). The process of proton hopping from one water molecule to the next, including the reorientation of the waters needed for proton transfer, is referred to as the Grotthuss mechanism. This hop-and-turn process provides a more rapid translocation of a proton than when transfer occurs solely by molecular diffusion. The reorganization of the hydrogen bonds between the water molecules after the translocation of the proton is the rate-limiting step. The proton transfer rates depend on the pK_a values of engaged acid/base pairs and reach higher values when the pK_as are matched (Pomès and Roux 1998). For both reasons, the transfer is slower if the proton transfer chain also contains hydrogen bond donors/acceptors from the protein itself (Pomès and Roux 1996, 1998; Decornez et al. 1999; Decoursey 2003).

In potato epoxide hydrolase StEH1, a proton wire-like structure has been identified, which could provide a route for the entry of the proton that is added to the anionic alkylenzyme intermediate during the catalytic cycle (Elfström and Widersten 2006). The protein-provided groups that coordinate the five water molecules of the hydrogen-bonding chain include backbone carbonyl oxygens and a histidyl imidazole (Fig. 2). In addition, Tyr^{149} and Tyr^{154} participate through their phenolic hydroxyls. The final member in the chain, Tyr^{154}, acts together with Tyr^{235} to provide the hydrogen bond donors needed to position the oxirane oxygen of the epoxide substrate. Such positioning allows efficient nucleophilic attack by Asp^{105}, which in turn leads to the formation of a covalent alkylenzyme intermediate. Mutation of either Tyr^{154} or Tyr^{235} to phenylalanine results in loss of activity (Elfström and Widersten 2005, 2006). A corresponding mutation of Tyr^{149}, by contrast, allowed for an additional water molecule to fill the available space and participate in the chain (Fig. 3), thereby maintaining efficient proton transfer and a catalytically competent enzyme. The observed increases in k_{cat}, however, (Table 2) are unlikely to primarily originate from a facilitated proton transport from solvent to Tyr^{154} for two reasons: (1) the intrinsic rates of proton transfer between electronegative atoms are expected to be much faster ($> 10^{10}$ s^{-1}) than the catalytic turnover numbers (< 300 s^{-1}); (2) the rate-limiting step in StEH1-catalyzed TSO hydrolysis is not protonation of the alkylenzyme, but rather its hydrolysis (Thomaeus et al. 2007). Hence, k_{cat} is mainly dictated by the energy barrier for the formation of the transition state of the hydrolytic half-reaction. If, however, protonation of the alkylenzyme facilitates the formation of this transition state, an increased value of k_{cat} for Y149F-catalyzed TSO hydrolysis would be expected. This could be due, for instance, to a reduction in the electrostatic repulsion that would otherwise exist in a doubly negatively-charged high-energy species. In essence, the determined rates of formation and hydrolysis of the alkylenzymes in the Y149F

mutant support these arguments. The increased values of k_2 and k_3 indicate that both proton transfer and alkylenzyme hydrolysis have been facilitated by the mutation.

The reactions with the two TSO enantiomers are affected differently by the mutations; the hydrolysis efficiency with the *S*,*S*-enantiomer is weakly enhanced by removal of the protein-water hydrogen bonds in the proton wire. These differences can be attributed to distinct characteristics of the hydrolysis of the two enantiomers. *S*,*S*-TSO is bound to the enzyme with higher affinity than is *R*,*R*-TSO (Elfström and Widersten 2005), so accumulation of the Michaelis complex contributes to K_M to a larger degree. In the *R*,*R*-TSO reaction, formation of the alkylenzyme is more efficient and exceeds hydrolysis rates by an order of magnitude, resulting in accumulation of the alkylenzyme. Hence, a facilitated alkylenzyme hydrolysis will under such circumstances also result in higher values of K_M. The observed changes in enantiospecificity are in any case noteworthy: mutations distant from the central catalytic residues that resulted in the loss of three protein-water hydrogen bonds caused a shift in enantiopreference exceeding 30-fold.

For the Y149F mutant the catalytic turnover numbers are increased for the respective enantiomers of TSO over the pH range from 5.1 to 7.9 (Fig. 5). This increase may reflect facilitation of product formation by lowering the activation energy for formation of the tetrahedral intermediate. We have previously reported that the pH dependence of k_{cat} in StEH1 can be explained by different protonation states of His^{300} with altering acidity through the catalytic cycle, presumably as an effect of the changing ionic states of the active site micro-environment (Thomaeus et al. 2007). The curvatures of the respective pH profiles for the *R*,*R*- and *S*,*S*-TSO reactions, however, do not indicate that major changes in the acidity of the catalytically important His^{300} have occurred as a result of the Y149F mutation (Fig. 5). Hence, the

observed increases in k_{cat} and K_M at pH 6.8 are probably not an effect of a change in rate limiting steps dependent on His^{300} protonation states.

Hydrogen bonds between protein and water molecules may contribute substantial stabilization to protein structure. In StEH1, the H153F and Y149F mutants lose one and two protein-water hydrogen bonding interactions, respectively, which appears to destabilize the structure. Removing three interactions in mutant Y149F/H153F (Figs. 2 and 6) is linked to a lowering of the half-life at 55 °C from 2.25 hours to 20 minutes. It should be noted, however, that the measured feature here is loss in catalytic activity rather than a direct analysis of structural unfolding.

A structure-based sequence alignment was used to compare the potato epoxide hydrolase and nine other plant epoxide hydrolases, and shows strong conservation of a tyrosyl residue corresponding to Tyr^{149} in StEH1 (Fig. 7). The residue is conserved in eight out of the ten plant epoxide hydrolases, a higher degree of conservation than seems to be required by the structural setting. The conservation thus supports the notion that a tyrosyl residue in this position may contribute its hydroxyl to the hydrogen bond chain of water molecules in many other plant species. By contrast, the histidyl residue at position 153 (in StEH1) is only conserved in the rice epoxide hydrolase; most other plant isoenzymes contain a tyrosyl residue in the corresponding position. Modeling of this mutation in the StEH1 structure indicates that the hydroxyl group of a tyrosine could replace the histidine imidazole moiety in the hydrogen bonding chain. Hydrogen-bonding capacity is thus a conserved feature at this position. The residues corresponding to Pro^{186}, Leu^{266} and His^{269} in StEH1 are reasonably well conserved although the contributions of these residues to the putative wire are *via* backbone oxygen interactions with the water molecules. The conservation seems to be based on the need to preserve the correct local structure, rather than a

more direct role. The observed patterns of residue conservation imply similar functions in other plant epoxide hydrolases, i.e. contributing to coordination of a water hydrogen bond chain.

The water channel in StEH1 seems to serve two functions: to act as a proton wire for efficient protonation of the alkylenzyme intermediate during catalysis, and to stabilize the enzyme structure through hydrogen bonding with protein side chains. Furthermore, the combination of the results from the present study with a previous report describing a plausible proton escape route out of the active site (Thomaeus et al. 2007), suggests that plant epoxide hydrolases may have evolved to efficiently supply and remove protons to the catalyzed reaction. While the exit route for protons appears to be structurally conserved also in mammalian epoxide hydrolases (Thomaeus et al. 2007) we have not been able to identify structural features in epoxide hydrolase crystal structures of mammalian (1VJ5, 1CQZ), bacterial (1EHY) or fungal (1Q07) origin that corresponds to the water entry channel found in the plant enzyme.

The His^{300} imidazole must exist in an unprotonated state in order to function as catalytic base. This relies on efficient proton transfer from the corresponding imidazolium, formed during the initial stages of the catalytic cycle, out of the active site. On the other hand, the anionic alkylenzyme intermediate requires protonation prior to its hydrolysis to form the diol product. Our analysis of the enzyme structure suggests that in plant enzymes both entrance and exit pathways for protons are integrated into the protein structure, forming a continuous path that runs from the surface of the protein to the buried active site then back to solvent (Fig. 8).

Materials and Methods

Site-directed mutagenesis

Mutants were constructed using polymerase chain reactions including mutagenic primers (Thermo Scientific) and plasmid pGTacStEH1-5H (Elfström and Widersten, 2005) coding for wild-type StEH1 as template. Mutant Y149F was constructed by substituting a TAT codon with a TTT at position 149 in the amplified cDNA. The H153F mutant was constructed by changing the codon CAT at position 153 in the cDNA for a TTT codon. The double mutant Y149F/H153F was constructed by introducing both codon substitutions at position 149 and 153 in the cDNA. The mutated cDNA fragments were subcloned between the *Mun*I and *Xho*I sites of pGTacStEH1-5H and the plasmid constructs were sequenced in full to confirm the mutations and ensure that no further alterations in the cDNAs had occurred.

Structure alignment

Sequences similar to StEH1 were identified using BLAST (Altschul et al. 1997). Structure-based sequence alignments were carried out using Indonesia (Madsen, Kleywegt and Johansson, unpublished computer program http://xray.bmc.uu.se/~dennis/).

Protein expression and purification

Expression plasmids encoding wild-type or mutant StEH1 were transformed into *E. coli* XL1-Blue bacteria by electroporation. Protein expression and purification of the His-tagged wild-type and mutant enzymes were performed as described earlier (Elfström and Widersten, 2005). Protein concentrations of collected fractions were determined from the absorbance values at 280 nm. The molar absorbance coefficients used, calculated from the respective amino acid compositions, were 59030 $M^{-1}cm^{-1}$

for wild type and mutant H153F, and 57630 $M^{-1}cm^{-1}$ for mutant Y149F and double mutant Y149F/H153F.

Crystallization of mutant Y149F

The Y149F mutant protein was crystallized by vapor diffusion in hanging drops of 2 μL protein and 2 μL reservoir solution (25% PEG 10000, 0.1 M HEPES, pH 7.5) at room temperature. Crystals (~0.1 x 0.05 x 1 mm^3) appeared within three days. Before being flash-cooled in liquid nitrogen, crystals were transferred to cryoprotectant comprised of 20% glycerol, 25% PEG 10000 and 0.1 M HEPES, pH 7.5. X-ray data were collected at beamline ID23 at the European Synchrotron Radiation Facility (ESFR), Grenoble. A data set of 99.6% completeness to 2 Å resolution was obtained. Diffraction data were indexed using MOSFLM (Leslie 1999) and processed with SCALA (Evans 1993) as implemented in the CCP4 interface (Potterton et al. 2003). The crystals possessed the symmetry of the space group $P2_12_12_1$. Statistics for the data set are shown in Table 1 (Engh and Huber 1991; Kleywegt and Jones 1996).

Structure determination and refinement of mutant Y149F

The structure of the mutant Y149F was solved by molecular replacement with MOLREP (Vagin and Teplyakov 1997). The search model included all protein atoms from the earlier 2 Å resolution wild-type structure [Protein Data Bank (Berman et al. 2002) entry code 2CJP (Mowbray et al. 2006)]. Two molecules were found in the asymmetric unit. The structure was refined by alternating cycles of refinement in REFMAC (Murshudov et al. 1997) and model rebuilding in 'O' (Jones et al 1991). Progressive inclusion of water molecules and a fragment of PEG, modeled as tetraethylene glycol, dropped the R-factor to 17.0 % (Rfree = 20.3%). Final

refinement statistics are given in Table 1. The final model and experimental diffraction data are deposited at the Protein Data Bank with entry code xxx.

Steady state kinetics and pH dependencies

The enzyme-catalyzed initial rates of TSO hydrolysis were determined in 0.1 M sodium phosphate, pH 6.8 at 30 ˚C. TSO was dissolved in acetonitrile and added to the reaction mixture, resulting in a final concentration of 1% (v/v) acetonitrile. The conversion from epoxide to diol was detected spectrophotometrically by measuring the decline in absorbance over time at 229 nm ($\Delta\varepsilon$ = -15 $mM^{-1}cm^{-1}$) (Wixtrom and Hammock 1988). Reactions were recorded for 20 to 60 seconds. Enzyme concentrations used in reactions were 25 nM, 26 nM and 50 nM, for mutants H153F, Y149F/H153F and Y149F, respectively. The concentrations of *R,R*-TSO or *S,S*-TSO were varied between 1.6 and 70 μM. At least three measurements at every substrate concentration were made. k_{cat}, K_M, and k_{cat}/K_M were determined by fitting the experimental data to the Michaelis-Menten equation in the MMFIT or RFFIT programs in SIMFIT (http://www.simfit.man.ac.uk). The pH dependence of k_{cat} for the Y149F mutant was determined in 0.1 M sodium phosphate in the pH range of 5.1-7.9 using the same substrate concentration range as well as enzyme concentration. The determined k_{cat} values were fitted to equation (1) with RRFIT.

$$L_H = \frac{\frac{[H^+]^2}{K_{a1}K_{a2}}L_{H_2A} + \frac{[H^+]}{K_{a2}}L_{HA^-} + L_{A^{2-}}}{1 + \frac{[H^+]}{K_{a2}} + \frac{[H^+]^2}{K_{a1}K_{a2}}} \qquad (1)$$

In Equation 1, describing a doubly ionizing system, L_H is the pH-dependent kinetic parameter k_{cat}. L_{H2A}, L_{HA-} and L_{A2-} are the respective amounts of the protonated and

deprotonated states of the enzyme-substrate complexes and K_{a1} and K_{a2} the respective apparent acid constants.

Pre-steady state kinetics

Microscopic rate constants and the equilibrium dissociation constant of ES (K_S) were determined by following the transient pre-steady state reaction phases in a SX20 stopped-flow spectrometer (Applied Photophysics Ltd, Leatherhead, UK). The reaction progresses were followed by recording the change in intrinsic tryptophan fluorescence of wild-type StEH1 and mutant Y149F during the reaction with either enantiomer of TSO. An excitation wavelength of 290 nm was used and the emitted fluorescence was detected after passing a 320 nm cut-off filter. The apparent rate constants were extracted by fitting a single exponential with floating endpoint to the detected fluorescence trace,

$$F = A \exp(-k_{obs}t) + C \quad (2)$$

where A is the amplitude of the fluorescence change, k_{obs} the observed rate and C the floating end point of the progression curve. Each k_{obs} used for parameter extraction was determined from the average of 8-12 reaction traces. The pre-steady state parameters, K_S, k_2, k_{-2} and k_3 were determined at enzyme concentrations of 0.5-4 μM with varying substrate concentrations in 0.1 M sodium-phosphate, pH 6.8, at 30 °C. The substrate-dependence of k_{obs} was plotted and fitted to Equation 3 with QNFIT in SIMFIT, allowing for determination of K_S, k_2 and $(k_{-2}+k_3)$. The individual values of $k_{-2}+k_3$ were determined from the expression of k_{cat} (Equation 4) inserting the values of k_2 and k_{cat}.

$$k_{obs} = \frac{k_2[S]}{K_S + [S]} + (k_{-2}+k_3) \quad (3)$$

$$k_{cat} = \frac{k_2 k_3}{(k_2 + k_{-2} + k_3)} \quad (4)$$

Thermostability

The remaining enzyme activities with 50 μM *R,R*-TSO in 0.1 M sodium phosphate, pH 6.8 at 30 ˚C were determined for the wild type and various mutants after pre-incubation at 55 ˚C. The enzyme concentrations used were 50 nM for wild type, 51 nM for the Y149F mutant, 25 nM for the H153F mutant, and 26 nM for the double mutant. Substrates were added to the reaction mixtures at a volume resulting in a final concentration of 1% (v/v) acetonitrile. Aliquots were withdrawn every half hour for activity measurements. The activity prior to incubation at 55 ˚C was set to 100% relative activity. To test for possible reversibility in inactivation, measurements on the Y149F mutant and the wild-type enzymes were performed every hour following a 3-hour incubation at 55 ˚C, followed by incubation at room temperature. At least three measurements for every incubation time point were made and three different enzyme samples were used for all variants. In addition, the thermostabilities of wild-type and Y149F mutant enzymes (50 nM concentrations) were analyzed after incubation at varying temperatures, 30 to 85 ˚C, for a defined period of time, 5 min. The remaining enzyme activities in the presence of 50 μM *R,R*-TSO in 0.1 M sodium phosphate, pH 6.8 were determined at 30 ˚C. Retained activity after incubations was expressed as per cent of enzyme activity determined prior to incubation.

Acknowledgements

The authors wish to thank Mattias Engman for assisting in purification of the TSO enantiomers. This work was supported by the Ingegerd Bergh and Carl Trygger

Foundations (MW) and by the Swedish Research Council (MW and SM). AT is a recipient of a stipend from the Lawski Foundation.

References

Altschul, S.F., Madden, T.L., Schaffer, A.A., Zhang, J., Zhang, Z., Miller, W. and Lipman, D.J. 1997. Gapped BLAST and PSI-BLAST: a new generation of protein database search programs. *Nucleic Acids Res*. **25:** 3389-3402.

Arand, M., Cronin, A., Oesch, F., Mowbray, S.L. and Jones, T.A. 2003. The telltale of epoxide hydrolases. *Drug Met. Rev.* **35:** 365-383.

Archelas, A. and Furtoss, R. 2001. Synthetic applications of epoxide hydrolases. *Curr. Opin. Chem. Biol.* **5:** 112-119.

Armstrong, R.N. and Cassidy, C.S. 2000. New structural and chemical insights into the catalytic mechanism of epoxide hydrolases. *Drug. Met. Rev.* **32:** 327-338.

Berman, H.M., Battistuz, T., Bhat, T.N., Bluhm, W.F., Bourne, P.E., Burkhardt, K., Feng, Z., Gilliland, G.L., Iype, L., Jain, S., Fagan, P., Marvin, J., Padilla, D., Ravichandran, V., Schneider, B., Thanki, N., Weissiq. H., Westbrook, J.D. and Zardecki, C. 2002. The Protein Data Bank. *Acta Crystallogr. D Biol. Crystallogr.* **58:** 899-907.

Decornez, H., Drukker, K. and Hammes-Schiffer, S. 1999. Solvation and hydrogen-bonding effects on proton wires. *J. Phys. Chem. A* **103:** 2891-2898.

Decoursey, T.E. 2003. Voltage-gated proton channels and other proton transfer pathways. *Physiol. Rev*. **83:** 475-579.

Elfström L.T. and Widersten, M. 2005. Catalysis of potato epoxide hydrolase, StEH1, *Biochem. J.* **390:** 633-640.

Elfström L.T. and Widersten, M. 2006. Implications for an ionized alkyl-enzyme intermediate during StEH1-catalyzed *trans*-stilbene oxide hydrolysis. *Biochemistry* **45:** 205-212.

Engh, R.A. and Huber, R. 1991. Accurate bond and angle parameters for X-ray protein structure refinement. *Acta Crystallogr*. **A47:** 392-400.

Evans, P.R. 1993. *Proceedings of CCP4 Study Weekend on Data Collection and Processing*, Warrington, England.

Fauth, M., Schweizer, O., Buchala, A., Markstädter, C., Riederer, M., Kato, T. and Kauss, H. 1998. Cutin monomers and surface wax constituents elicit H_2O_2 in conditioned cucumber hypocotyl segments and enhance the activity of other H_2O_2 elicitors. *Plant Physiol.* **117:** 1373-1380.

Frank, R.A.W., Titman, C.M., Pratap, J.V., Luisi, B.F and Preham, R.N. 2004. A molecular switch and proton wire synchronize the active sites in thiamine enzymes. *Science* **306:** 872-876.

Imig, J.D. 2005. Epoxide hydrolase and epoxygenase metabolites as therapeutic targets for renal diseases. *Am. J. Physiol. Renal Physiol.* **289:** 496-503.

Jones, T.A., Zou, J.-Y., Cowan, S.W. and Kjeldgaard, M. 1991. Improved methods for building protein models in electron density maps and the location of errors in these models. *Acta Crystalllogr*. **A47:** 110-119.

Kleywegt, G.J. and Jones, T.A. 1996 Phi/Psi-cology: Ramachandran revisited. *Structure* **4:** 1395-1400.

Koeller, K.M. and Wong, C.-H. 2001. Enzymes for chemical synthesis. *Nature* **409:** 232-240.

Kolattukudy, P.E. 1981. Structure, biosynthesis, and biodegradation of cutin and suberin. *Ann. Rev. Plant Physiol.* **32:** 539-567.

Leslie, A.G. 1999. Integration of macromolecular diffraction data. *Acta Crystallogr*. **D55:** 1696-1702.

Morrisseau, C. and Hammock, B.D. 2005. Epoxide hydrolases: mechanisms, inhibitor designs and biological roles. *Annu. Rev. Pharmacol. Toxicol.* **45:** 311-333.

Mowbray, S.L., Elfström, L.T., Ahlgren, K.M., Andersson, C.E. and Widersten, M. 2006. X-Ray structure of potato epoxide hydrolase sheds light on substrate specificity in plant enzymes. *Protein Sci.* **15:** 1628-1637.

Murshudov, G.N., Vagin, A.A. and Dodson, E.J. 1997. Refinement of macromolecular structures by the maximum-likehood method. *Acta Crystallogr*. **D53:** 240-255.

Nagle, J.F. and Morowitz, H.J. 1978. Molecular mechanisms for proton transport in membranes. *Proc. Natl. Acad. Sci. USA* **75:** 298-302.

Ollis, D.L., Cheah, E., Cygler, M., Dijkstra, B., Frolow, F., Franken, S.M., Harel, M., Remington, S.J., Silman, I., Schrag, J., Sussman, J.L., Verschueren, K.H.G. and Goldman, A. 1992. The α/β hydrolase fold. *Protein Eng.* **5:** 197-211.

Pomès, R. and Roux, B. 1996. Structure and dynamics of a proton wire: a theoretical study of H^+ translocation along the single-file water chain in the Gramicidin A channel. *Biophys. J.* **71:** 19-39

Pomès, R. and Roux, B. 1998. Free energy profiles for H^+ conduction along hydrogen-bonded chains of water molecules. *Biophys. J.* **75:** 33-40.

Potterton, E., Briggs, P., Turkenburg, M. and Dodson, E. 2003. A graphical user interface to the CCP4 program suite. *Acta Crystallogr*. **D59:** 1131-1137.

Read, R.J. 1986. Improved Fourier coefficients for maps using phases from partial structures with errors. *Acta Crystallogr*. **A42:** 140-149.

Schmelzer, K.R., Kubala, L., Newman, J.W., Kim, I.-H., Eiserich, J.P. and Hammock, B.D. 2005. Soluble epoxide hydrolase is a therpeutic target for acute inflammation. *Proc. Natl. Acad. Sci. USA* **102:** 9772-9777.

Steinreiber, A. and Faber, K. 2001. Microbial epoxide hydrolases for preparative biotransformations. *Curr. Opin. Biotechnol.* **12:** 552-558.

Thomaeus, A., Carlsson, J., Åqvist, J. and Widersten, M., 2007. Active site of epoxide hydrolases revisited: a noncanonical residue in potato StEH1 promotes both formation and breakdown of the alkylenzyme intermediate. *Biochemistry* **46:** 2466-2479.

Vagin, A. and Teplyakov, A. 1997. MOLREP: an automated program for molecular replacement. *J. Appl. Cryst.* **30:** 1022-1025.

Wixtrom, R.N. and Hammock B.D. 1988. Continuous spectrophotometric assays for cytosolic epoxide hydrolase. *Anal. Biochem.* **174:** 291-299.

Zhang W., Koerner, I.P., Noppens, R., Grafe M., Tsai, H.-J., Morisseau, C., Luria, A., Hammock, B.D., Falck, J.R. and Alkayed N.J. 2007. Soluble epoxide hydrolase: a novel therapeutic target in stroke. *J. Cereb. Blood Flow Metab.* doi: 10.1038/sj.jcbfm.9600494.

Zhao, X., Yamamoto, T., Newman, J.W., Kim, I.-H., Watanabe, T., Hammock, B.D., Stewart, J., Pollock, J.S., Pollock, D.M. and Imig, J.D. 2004. Soluble epoxide hydrolase inhibition protects the kidney from hypertension-induced damage. *J. Am. Soc. Nephrol.* **15:** 1244-1253.

Table 1. Data Collection and Refinement Statistics.

Data collection statistics	Y149F mutant
Data collection beamline/detector	ESRF ID23:1/ADSC scanner
Cell axial lengths (Å)	55.9, 96.7, 122.2
Resolution range (Å)	20.0 - 2.0 (2.1 - 2.0)
Number of reflections measured	182,925
Number of unique reflections	45,424
Average multiplicity	4.0
Completeness (%)	99.6 (99.5)
Rmeas (%)	11.3, (18.1)
> >	*11.6 (8.0)*
Refinement statistics	
Resolution range (Å)	*20.0 - 2.0*
Number of reflections used in working set	*43,049*
No. of reflections for Rfree calculation	*2152*
R-value, Rfree (%)	*17.0, 20.3*
No. of non-hydrogen atoms	*5780*
No. of solvent waters	*654*
Mean B-factor, protein atoms, A and B molecules (Å^2)	*11.8, 14.5*
Mean B-factor, solvent atoms (Å^2)	*26.4*
Mean B-factor, tetraethylene glycol atoms, A molecule (Å^2)	*32.3*
Ramachandran plot outliers (%)[a]	*1.7*
r.m.s. deviation from ideal bond length (Å)[b]	*0.008*
r.m.s. deviation from ideal bond angle (°)[b]	*1.03*

The space group is $P2_12_12_1$. Information in parentheses refers to the highest resolution shell.

[a] *Calculated using a strict-boundary Ramachandran plot (Kleywegt and Jones 1996).*

[b] *Using the parameters of Engh and Huber (1991).*

Table 2. *Steady state kinetic parameters of TSO hydrolysis catalyzed by wild-type StEH1, mutant Y149F, mutant H153F, and mutant Y149F/H153F at pH 6.8.*

	substrate					
	R,R-TSO			*S,S-TSO*		
	k_{cat}	K_M	k_{cat}/K_M	k_{cat}	K_M	k_{cat}/K_M
enzyme	*(s^{-1})*	*(μM)*	*($s^{-1}\mu M^{-1}$)*	*(s^{-1})*	*(μM)*	*($s^{-1}\mu M^{-1}$)*
wild type	*23±2*[a]	*10±1*[a]	*2.4±0.2*[a]	*3.8±0.1*[b]	*4.7±0.5*[b]	*0.80±0.07*[b]
Y149F	*44±2*	*36±3*	*1.2±0.06*	*6.8±0.4*	*6.8±0.9*	*1.04±0.09*
H153F	*15±2*	*94±20*	*0.16±0.01*	*12±1*	*11±1*	*1.1±0.1*
Y149F/H153F	*n.d.*	*n.d*	*0.20±0.01*	*12±1*	*5.2±0.5*	*2.2±0.2*

[a] *Data adapted from Elfström and Widersten (2005).* [b] *Data adapted from Thomaeus et al. (2007). n.d., Not determined due to inability to reach saturation within the solubility range of the substrate.*

Table 3. *Kinetic parameters of TSO hydrolysis catalyzed by wild-type StEH1 and mutant Y149F at pH 6.8.*

enzyme	*substrate*	K_S *(μM)*	k_2 (s^{-1})	k_2/K_S $(s^{-1}\ \mu M^{-1})$	k_{-2} (s^{-1})	k_3 (s^{-1})
wild type	*R,R-TSO*	*36±22*	*260±56*	*2.7±0.3*[a]	*16±18*	*24±3*[a]
Y149F	*R,R-TSO*	*500±900*	*300±400*	*0.80±0.60*	*30*	*60*
wild type	*S,S-TSO*	*11±6*[a]	*18±2*[a]	*1.8±1.4*[a]	*14±2*[a]	*3.2±0.06*[a]
Y149F	*S,S-TSO*	*15±7.9*	*40±4.0*	*4.9±2.3*	*21±2.4*	*12±1.8*

[a] *Data adapted from Elfström and Widersten (2005).*

Figure legends

Figure 1. *Kinetic mechanism of StEH1 catalyzed hydrolysis of TSO.*

Figure 2*. Schematic overview of the putative proton wire in StEH1.*

Figure 3. *Active site and hydrogen bond chain. (A) Residues in the active site of the Y149F mutant are shown together with the chain of waters that compose the putative proton wire. Electron density from a SIGMAA-weighted* $|2Fobs-Fcalc|$ *map (Read 1986) is shown contoured at a level of 1*σ*. Residues participating in catalysis (*Tyr^{154}*,* Tyr^{235}*,* Asp^{105} *and* His^{153}*), as well as the mutated* Phe^{149}*, are labeled. (B) The same residues and equivalent water molecules from the wild-type enzyme (shown in white) are superimposed, and the site of mutation indicated. Replacing* Tyr^{149} *with phenylalanine results in a change of the position in the closest water molecule.*

Figure 4. *Substrate concentration dependence of observed rates (*k_{obs}*) of alkylenzyme formation. Filled squares, R,R-TSO, filled circles, S,S-TSO. Solid lines represent the fits of Equation 3 to the observed rates.*

Figure 5. *pH dependence of* k_{cat}*. Effect of pH on the catalytic turnover,* k_{cat}*, for wild-type StEH1 catalyzed (unfilled square), mutant Y149F catalyzed (filled squares) reactions with R,R-TSO and the effect of pH on* k_{cat} *for wild-type StEH1 catalyzed (unfilled circles) and mutant Y149F catalyzed (filled circles) reactions with S,S-TSO. Lines represent the fits of Equation 1 to the experimental data. Error bars represent the standard error of* k_{cat}^{obs}*. Data for* $k_{cat}^{R,R\text{-}TSO}$ *and* $k_{cat}^{S,S\text{-}TSO}$ *with wild-type StEH1 were adapted from Elfström L. T. & Widersten, M. (2005).*

Figure 6. *Thermal inactivation of enzyme activity. Effect of incubation at 55 °C over time on the activity with 50 μM R,R-TSO with wild-type StEH1 (square), mutant Y149F (circle), mutant H153F (diamond), and mutant Y149F/H153F (triangle). Activities prior to incubation at 55 °C were normalized to 100%. (B) Remaining enzyme activities with R,R-TSO (50 μM) after five minute incubations at temperatures between 50 to 70 °C. Wild-type StEH1 (square) and mutant Y149F (circle). Activities prior to incubations at elevated temperatures were normalized to 100%.*

Figure 7. *Sequence alignment of soluble plant epoxide hydrolases. Regions of interest for the putative proton wire are shown; residues directly participating are indicated by white letters on black background. StEH1 (Swiss-Prot entry Q41415_SOLTU), soybean (Q39856_SOYBN), rough lemon (Q76E11_9ROSI), rape (Q8L5G6_BRANA), rice (Q9S7P1_ORYSA), pineapple (Q8H289_ANACO), E. lagascae (Q84ZZ3_EUPLA), barrel medic (A2Q320_MEDTR), chickpea (Q8LPE6_CICAR), mouse-ear cress (Q42566_ARATH).*

Figure 8. *Possible lateral proton translocation in StEH1. The gray arrow indicates the possible entrance and exit pathways for protons in and out of the active site. The side-chains of residues* Tyr^{149} *and* His^{153} *and water molecules facilitate proton transfer into the active site (high-lighted by a dotted circle) and the catalytic residue* Tyr^{154}*. From the active site, a chain of hydrogen bonds, consisting of a water molecule, and the side-chain groups of* Glu^{35}*,* Ser^{39}*,* Tyr^{219}*,* Arg^{41}*, and* Glu^{215}*, links the active site with bulk solvent and allows for the liberation of a proton at the other face of the enzyme.*

Fig. 1

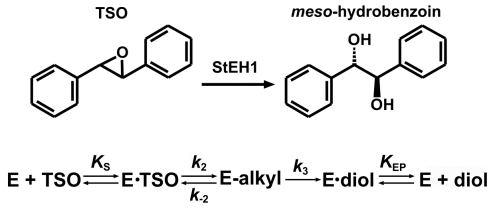
TSO
meso-hydrobenzoin
StEH1
OH
OH
E + TSO
E·TSO
E-alkyl
E·diol
E + diol

Fig. 2

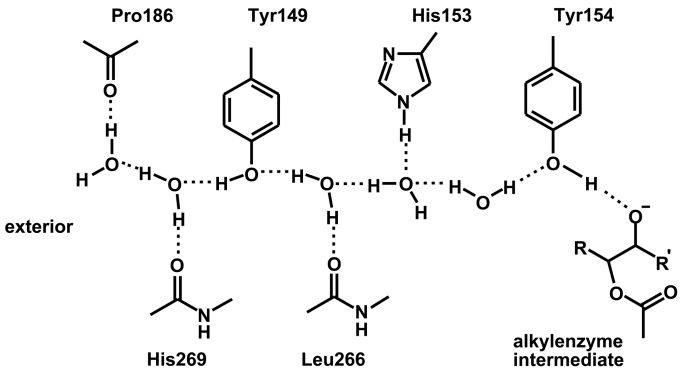
Pro186
Tyr149
His153
Tyr154
exterior
His269
Leu266
alkylenzyme
intermediate

Fig. 3

A

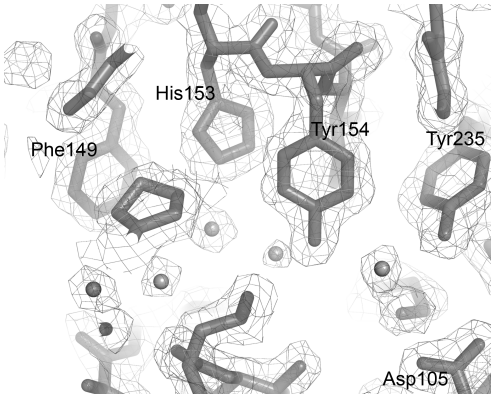
His153
Tyr154
Tyr235
Phe149
Asp105

B

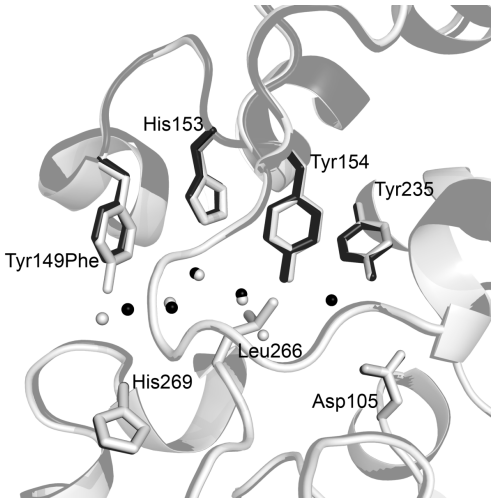
His153
Tyr154
Tyr235
Tyr149Phe
Leu266
His269
Asp105

Fig. 4

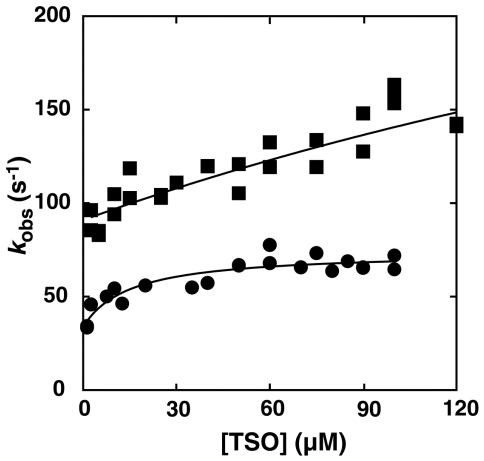
200
150
100
50
0
k_{obs} (s^{-1})
0
30
60
90
120
[TSO] (μM)

Fig. 5

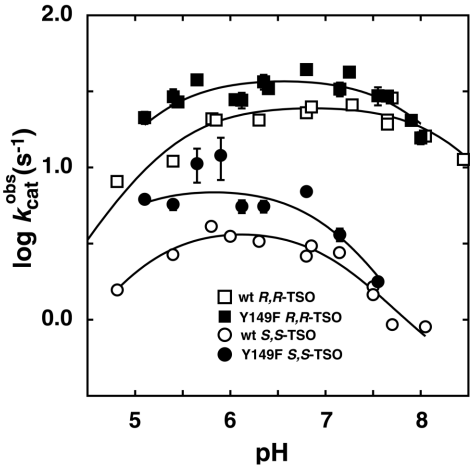
2.0
1.0
0.0
log k_{cat}^{obs} (s^{-1})
wt *R,R*-TSO
Y149F *R,R*-TSO
wt *S,S*-TSO
Y149F *S,S*-TSO
5
6
7
8
pH

Fig. 6

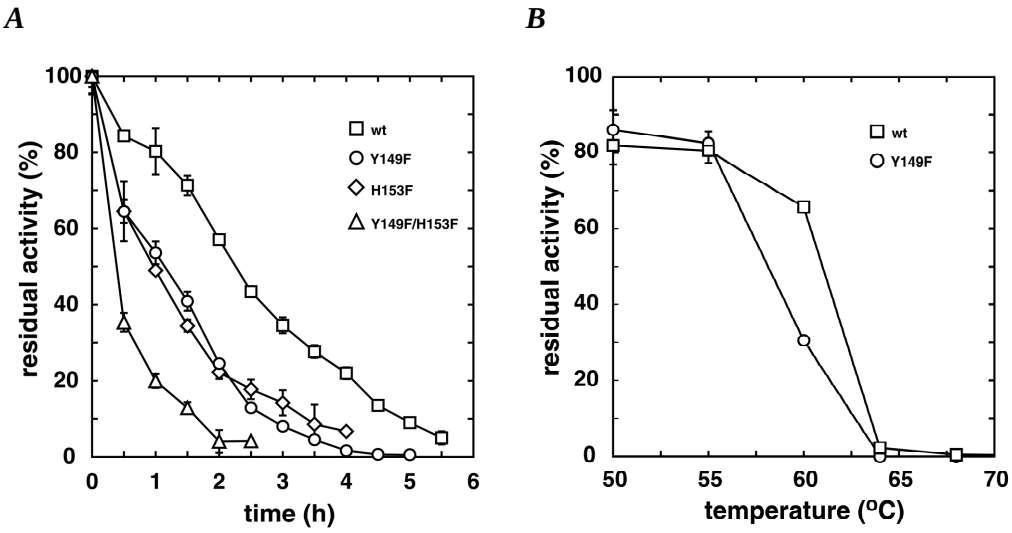

Fig. 7

StEH1	146KAIYGEDHYIS156	183YRDPAPF189	263EFDLVYHIPG272
soybean	142RALYGDDYYVC152	179TRNPGPP185	258ELDMVYNSLN267
rough lemon	142RAVYGDDYYIC152	179LRIPKPL185	258DQDLVYNNKG267
rape	143RKFYGDDFYMC153	180YRTPRPL186	260EQDLVYHFPG269
rice	147RAVCGDGHYIC157	184MRKAAPL190	264DQDLTYNIPG273
pineapple	145KHLYGDNIYVC155	182MRDPRPS188	260DLDLTYHYPN269
E. lagascae	147RKELGEDFYIC157	184SRHIRPP190	263DQDATYHLPG272
barrel medic	143RAAYGDDYYIC153	180TRKTGPP186	261DLDMVYTSPH270
chickpea	99RAAYGDDYYIC109	136TRKTGPP142	217ELDMVYTSLN226
mouse-ear cress	146RAFYGDDYYIC156	183YRTPGPV189	263ELDLVYYMPG272

Fig. 8

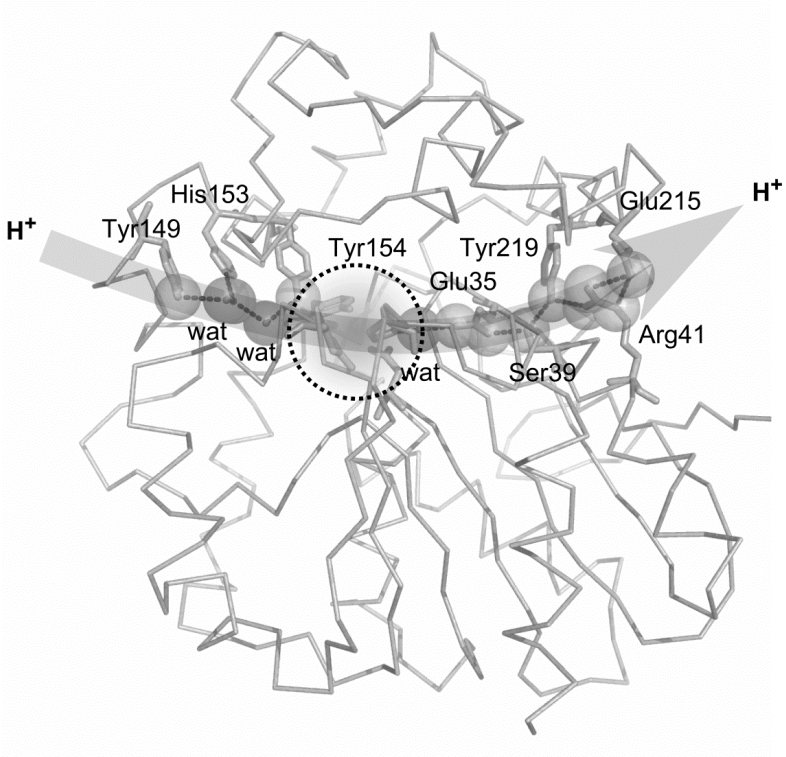
H+
His153
Tyr149
Tyr154
Tyr219
Glu215
H+
Glu35
wat
wat
wat
Arg41
Ser39

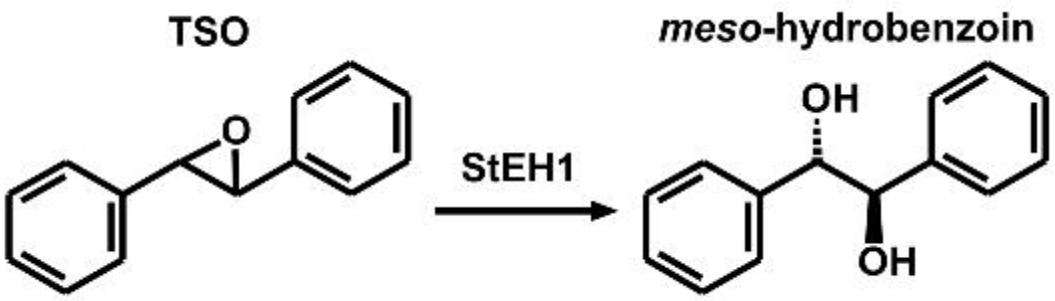

$$E + TSO \underset{}{\overset{K_S}{\rightleftharpoons}} E{\cdot}TSO \underset{k_{-2}}{\overset{k_2}{\rightleftharpoons}} E\text{-alkyl} \xrightarrow{k_3} E{\cdot}diol \overset{K_{EP}}{\rightleftharpoons} E + diol$$

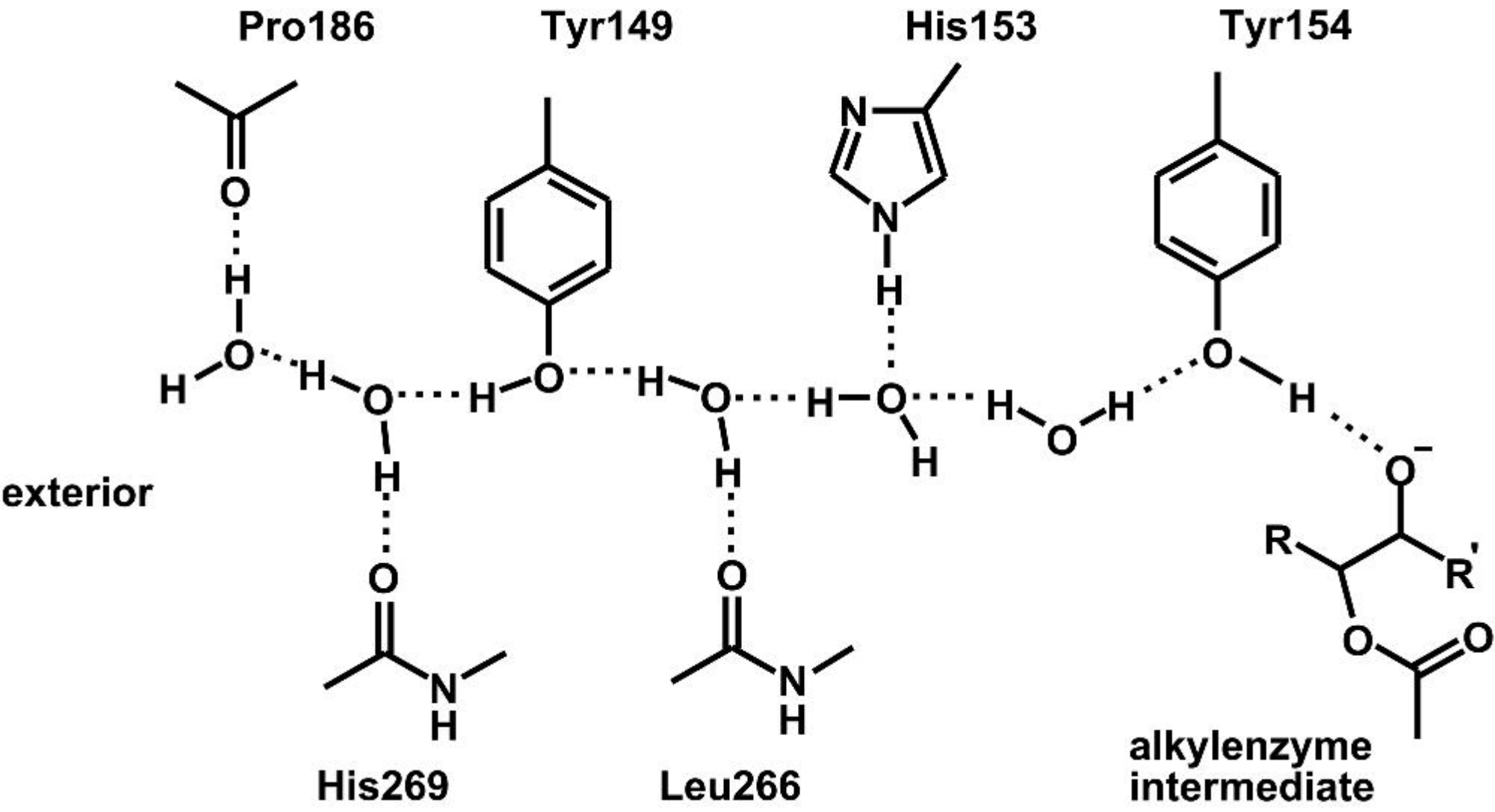
Pro186
Tyr149
His153
Tyr154
exterior
His269
Leu266
alkylenzyme
intermediate

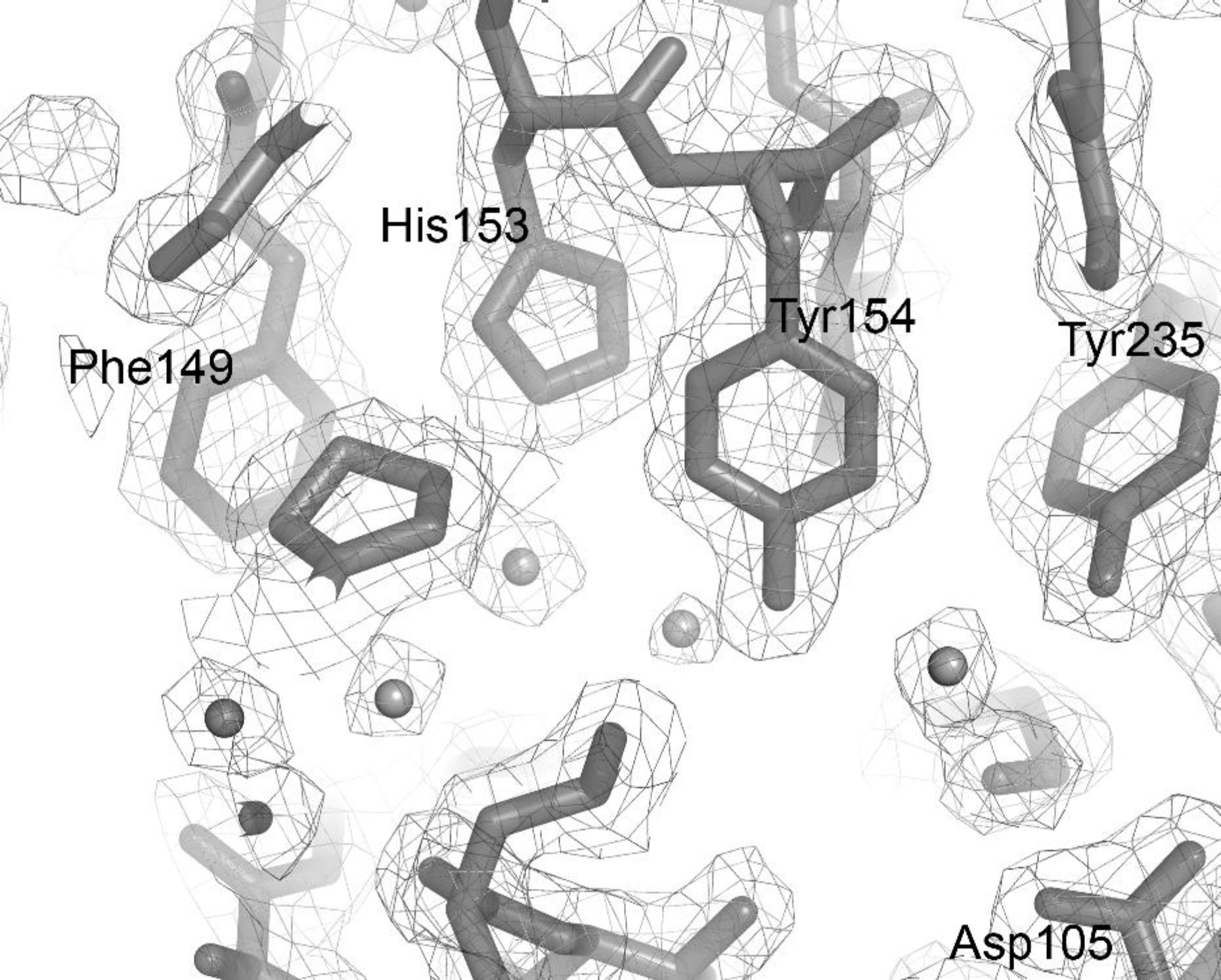
His153
Tyr154
Tyr235
Phe149
Asp105

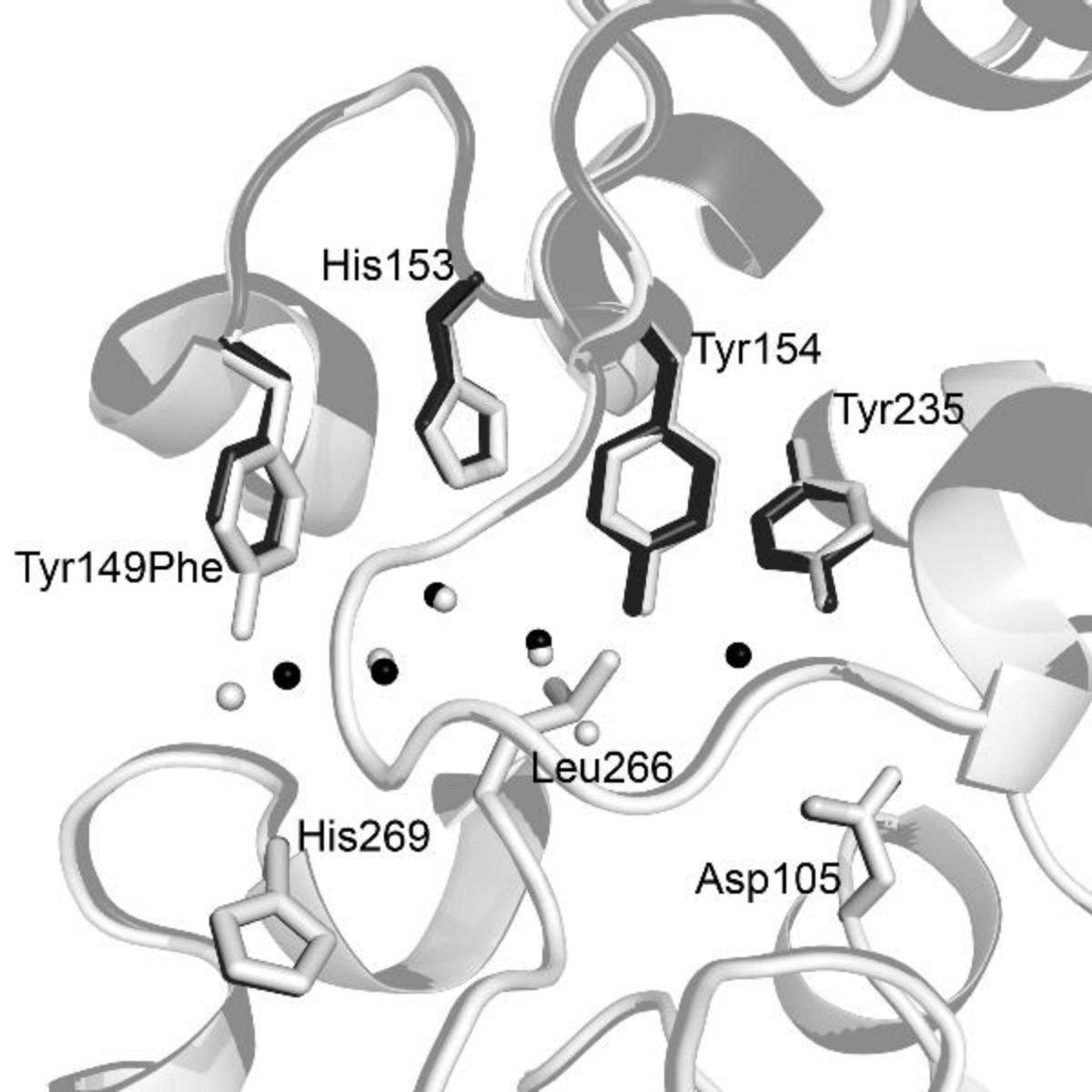
His153
Tyr154
Tyr235
Tyr149Phe
Leu266
His269
Asp105

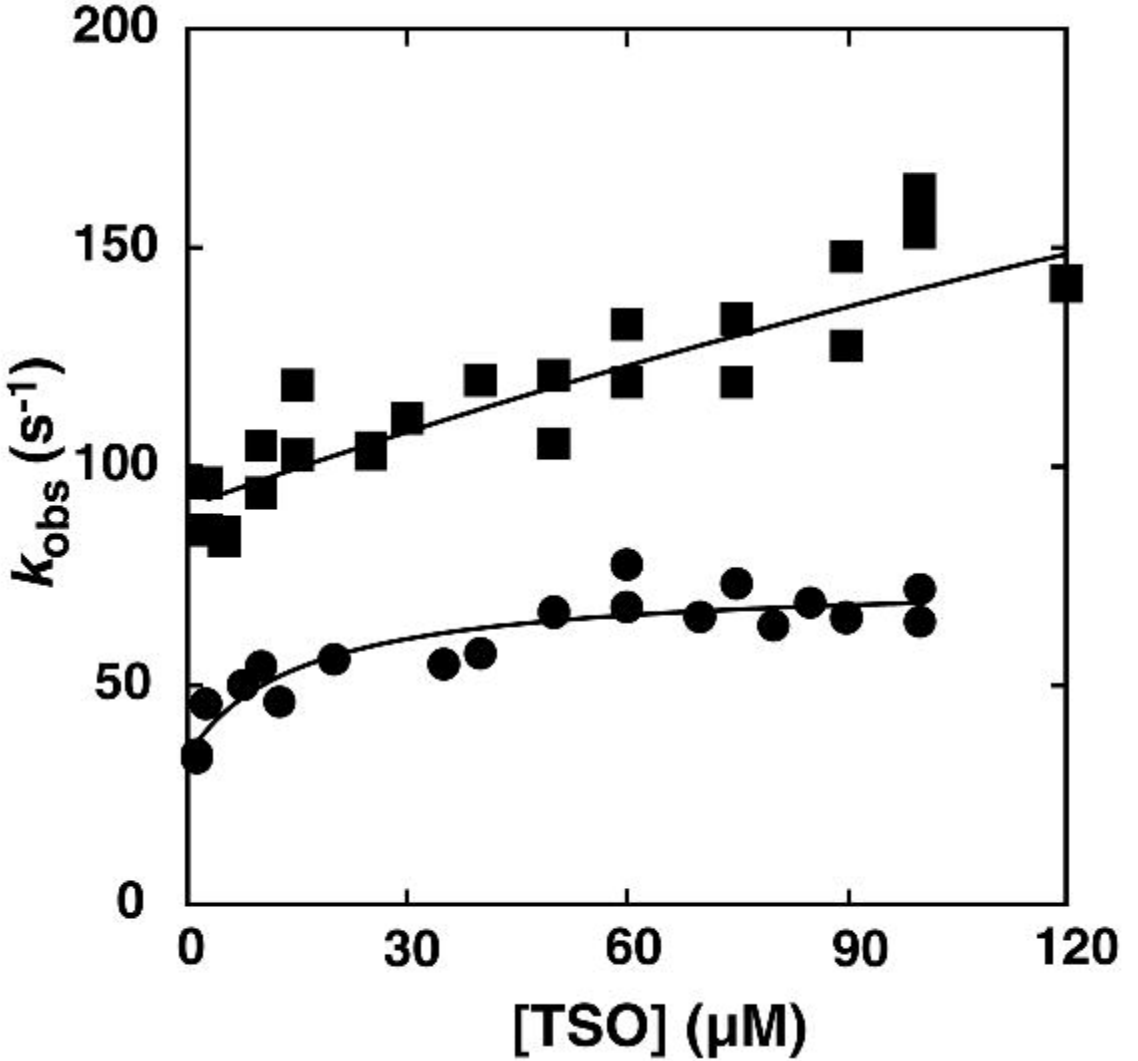
200
150
100
50
0
k_{obs} (s^{-1})
0
30
60
90
120
[TSO] (μM)

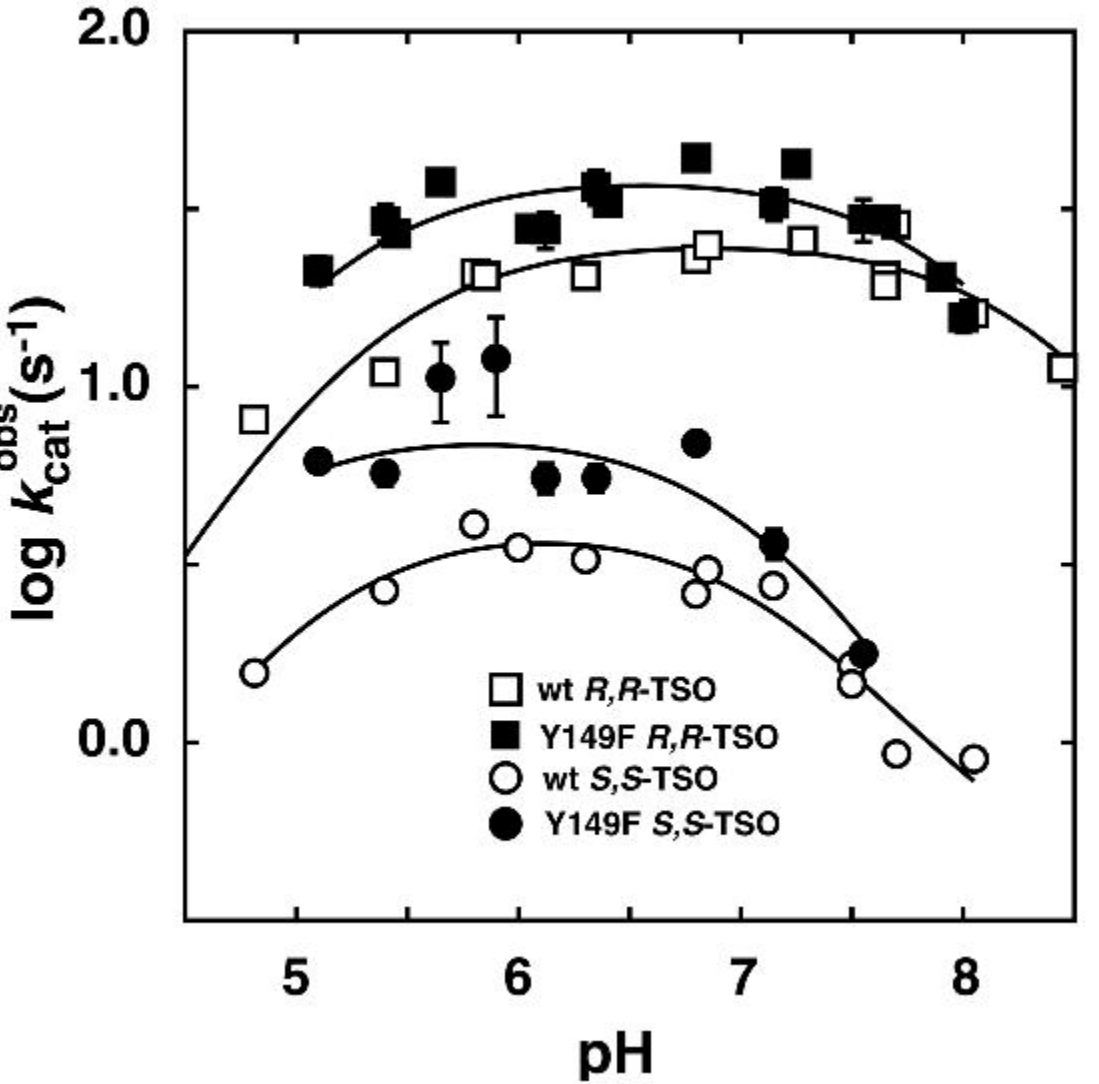
2.0
1.0
0.0
log k_{cat}^{obs} (s^{-1})
5
6
7
8
pH
wt *R,R*-TSO
Y149F *R,R*-TSO
wt *S,S*-TSO
Y149F *S,S*-TSO

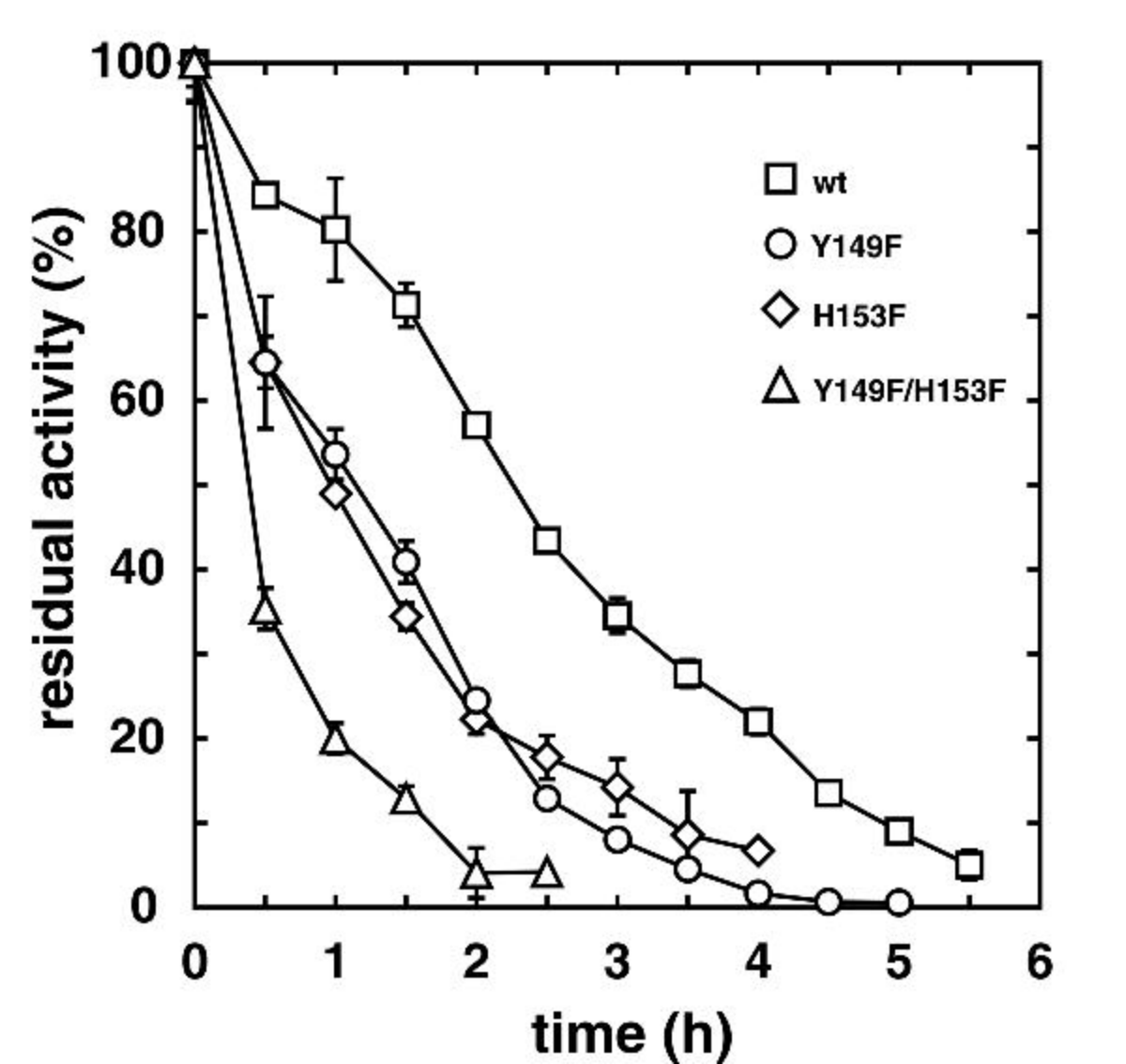
100
80
60
40
20
0
residual activity (%)
0
1
2
3
4
5
6
time (h)
wt
Y149F
H153F
Y149F/H153F

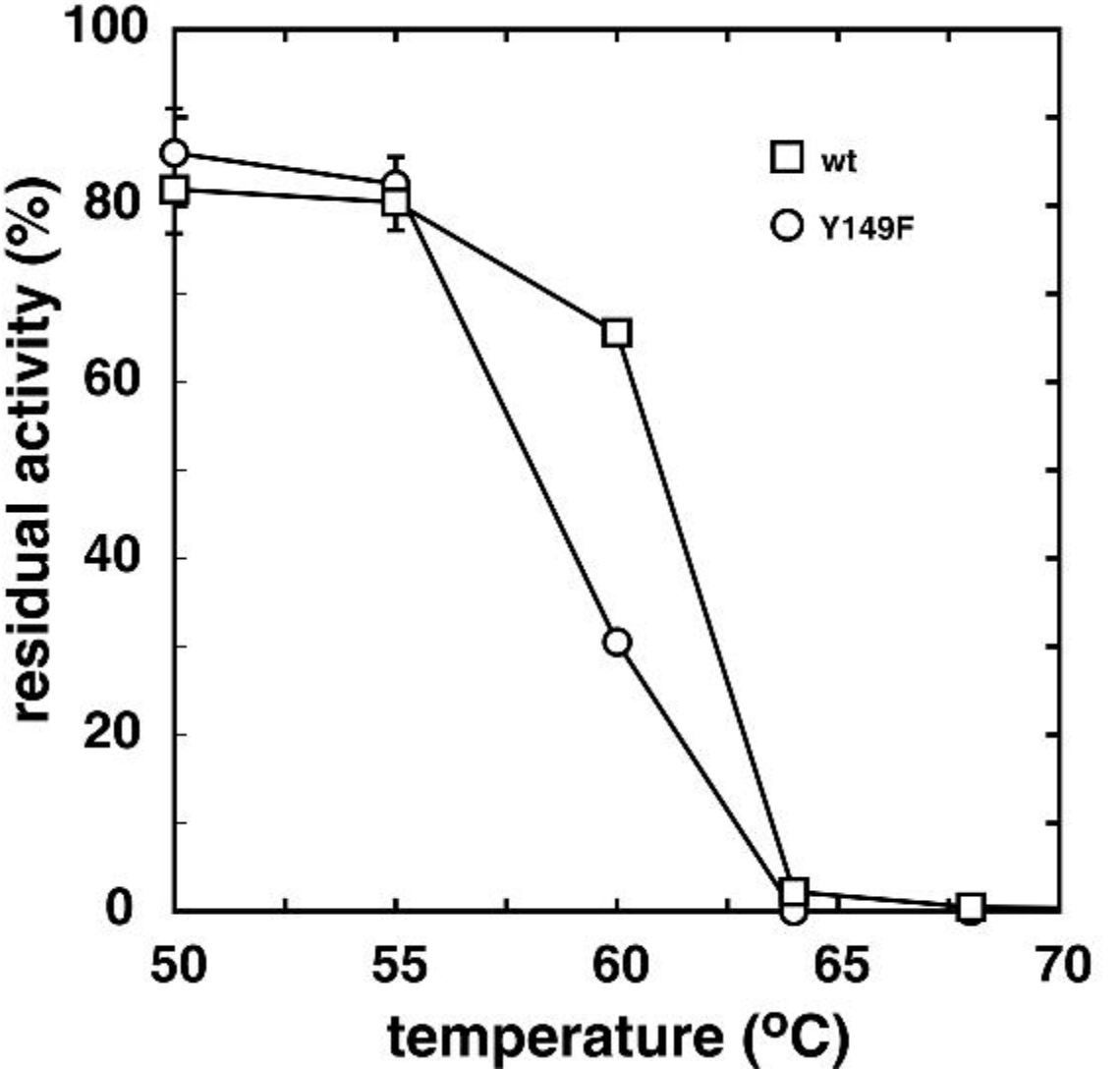
100
80
60
40
20
0
residual activity (%)
50
55
60
65
70
temperature (°C)
wt
Y149F

StEH1 146 KAIYGEDHYIS 156 183 YRDPAPF 189 263 EFDLVYHIPG 272
soybean 142 RALYGDDYYVC 152 179 TRNPGPP 185 258 ELDMVYNSLN 267
rough lemon 142 RAVYGDDYYIC 152 179 LRIPKPL 185 258 DQDLVYNNKG 267
rape 143 RKFYGDDFYMC 153 180 YRTPRPL 186 260 EQDLVYHFPG 269
rice 147 RAVCGDGHYIC 157 184 MRKAAPL 190 264 DQDLTYNIPG 273
pineapple 145 KHLYGDNIYVC 155 182 MRDPRPS 188 260 DLDLTYHYPN 269
E. lagascae 147 RKELGEDFYIC 157 184 SRHIRPP 190 263 DQDATYHLPG 272
barrel medic 143 RAAYGDDYYIC 153 180 TRKTGPP 186 261 DLDMVYTSPH 270
chickpea 99 RAAYGDDYYIC 109 136 TRKTGPP 142 217 ELDMVYTSLN 226
mouse-ear cress 146 RAFYGDDYYIC 156 183 YRTPGPV 189 263 ELDLVYYMPG 272

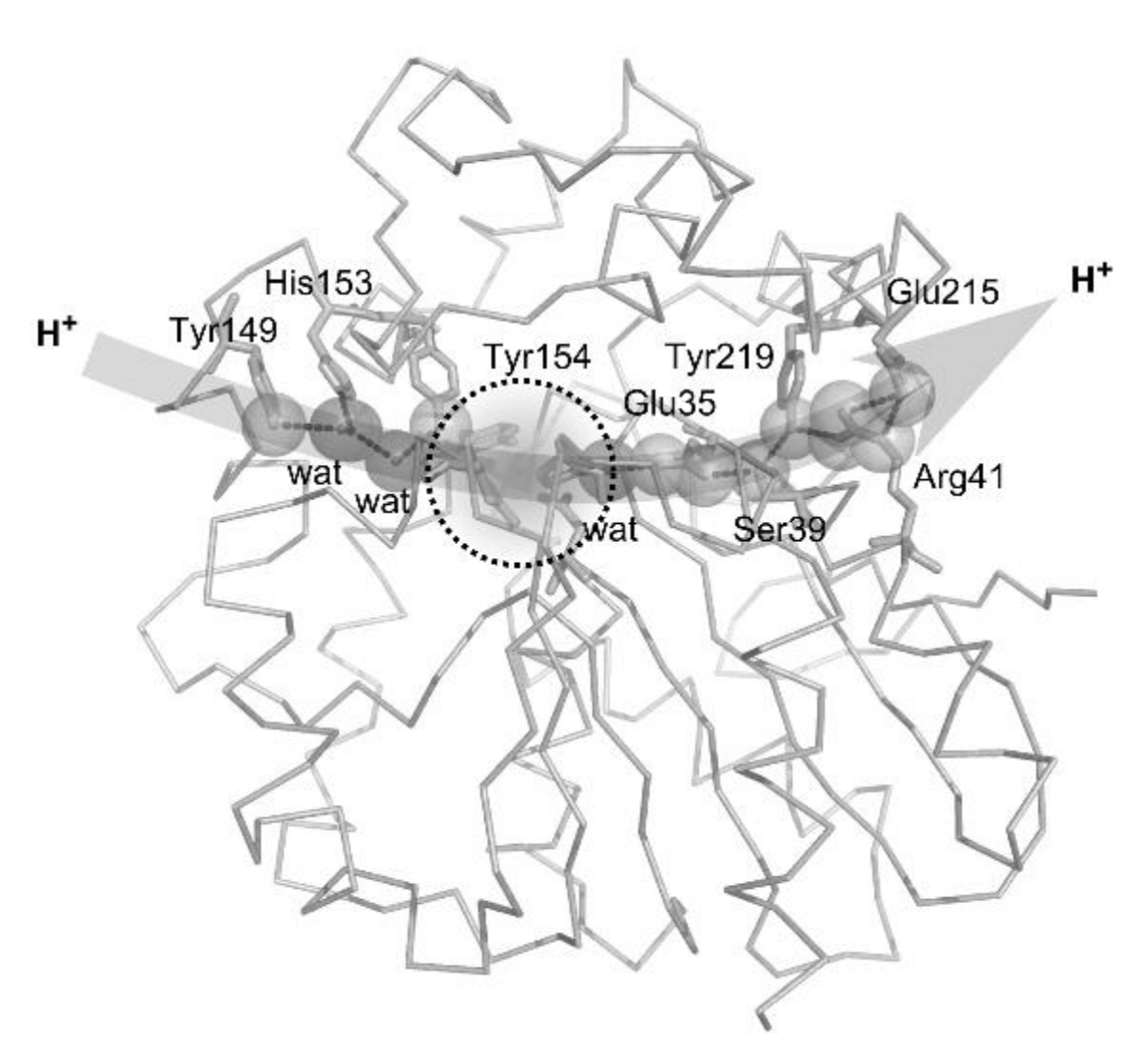
H+
His153
Tyr149
Tyr154
Tyr219
Glu215
H+
Glu35
wat
wat
wat
Arg41
Ser39